pest–plant cycles or even single-species dynamics with second-order delays such as maternal effects, which lead to periods of over $6T$ (ref. 24). The last would increase the prevalence of single-species dynamics.

Scaled period, τ, was calculated by dividing the period (in years) by time to maturity (in years), T_C (sources in Supplementary Information 3). For cases in which $\tau > 4$, we then asked if the cycle period in years exceeded $4T_C + 2T_R$; in series involving lynx (average maturation time = 1.5 years) this sum was eight years; in all others, where consumer and resource species develop in one year, it was six. Because maturation times and cycle periods are approximations, estimates of τ were rounded to the nearest integer. Periods with $\tau = 1$ were assigned to single-generation cycles; those with $2 \leq \tau \leq 4$ were assigned to delayed-feedback cycles.

The series were analysed 'blind', without knowledge of the species name or trophic role. We used multitaper spectral analysis[25,26] using the algorithm described in ref. 27. This technique avoids the often arbitrary choice of data tapering by using a series of optimal slepian tapers. We classified a series as periodic if there was both a clear peak in the power spectrum (of either the transformed or the untransformed data) and the corresponding P-value was <0.05. If there were missing values, we analysed the longest continuous segment of the data. If, upon visual inspection, only part of the series appeared cyclic, we analysed that segment. We analysed the data both with and without a logarithmic transformation, and removed any linear trend in both cases. If several series were available from any given area and time period, we analysed only one series, and only the predator if predator and prey series were available.

Received 30 October 2001; accepted 5 March 2002.

1. Lotka, A. J. *Elements of Physical Biology* (Dover, New York, 1925, reprinted 1956).
2. Hassell, M. P., Lawton, J. H. & May, R. M. Patterns of dynamical behaviour in single species populations. *J. Anim. Ecol.* **45,** 471–486 (1976).
3. Gurney, W. S. C. & Nisbet, R. M. *Ecological Dynamics* (Oxford Univ. Press, New York, 1998).
4. McCauley, E., Nisbet, R. M., De Roos, A. M., Murdoch, W. W. & Gurney, W. S. C. Structured population models of herbivorous zooplankton. *Ecol. Monogr.* **66,** 479–501 (1996).
5. Persson, L. *et al.* Ontogenetic scaling of foraging rates and the dynamics of a size-structured consumer-resource model. *Theor. Popul. Biol.* **54,** 270–293 (1998).
6. Briggs, C. J., Nisbet, R. M. & Murdoch, W. W. Host age-specific parasitoid gain, delayed-feedback, and multiple attractors in a host-parasitoid model. *J. Math. Biol.* **38,** 317–345 (1999).
7. Kendall, B. E. *et al.* Why do populations cycle? A synthesis of statistical and mechanistic modeling approaches. *Ecology* **80,** 1789–1805 (1999).
8. Kendall, B. E., Prendergast, J. & Bjornstad, O. N. The macroecology of population dynamics: taxonomic and biogeographic patterns in populations cycles. *Ecol. Lett.* **1,** 160–164 (1998).
9. Stenseth, N. C., Falck, W., Bjornstad, O. N. & Krebs, C. J. Population regulation in snowshoe hare and Canadian lynx: Asymmetric food web configurations between hare and lynx. *Proc. Natl Acad. Sci. USA* **94,** 5147–5152 (1997).
10. Bjornstad, O. N., Sait, S. M., Stenseth, N. C., Thompson, D. J. & Begon, M. The impact of specialized enemies on the dimensionality of host dynamics. *Nature* **409,** 1001–1006 (2001).
11. Gurney, W. S. C. & Nisbet, R. M. Fluctuation periodicity, generation separation, and the expression of larval competition. *Theor. Popul. Biol.* **28,** 150–180 (1985).
12. Jones, A. E., Nisbet, R. M., Gurney, W. S. C. & Blythe, S. P. Period to delay ratio near stability boundaries for systems with delayed feedback. *Math. Anal. Appl.* **135,** 354–368 (1988).
13. Blythe, S. P., Nisbet, R. M. & Gurney, W. S. C. Instability and complex dynamical behaviour in population models with long time delays. *Theor. Popul. Biol.* **22,** 147–176 (1982).
14. Higgins, K., Hastings, A. & Botsford, L. W. Density dependence and age structure: Nonlinear dynamics and population behaviour. *Am. Nat.* **149,** 247–269 (1997).
15. Nisbet, R. M. & Bence, J. R. Alternative dynamic regimes for canopy-forming kelp: A variant on density-vague population regulation. *Am. Nat.* **134,** 377–408 (1989).
16. Lauwerier, H. A. & Metz, J. A. J. Hopf bifurcation in host-parasitoid models. *Inst. Math. Appl. J. Math. Appl. Med. Biol.* **3,** 191–210 (1986).
17. Nisbet, R. M. & Gurney, W. S. C. *Modelling Fluctuating Populations* (Wiley, New York, 1982).
18. NERC Centre for Population Biology, Imperial College The Global Population Dynamics Database, (NERC, Ascot 1999); available at http://www.sw.ic.ac.uk/cpb/cpb/gpdd.html.
19. Finerty, J. P. *The Population Ecology of Cycles in Small Mammals: Mathematical Theory and Biological Fact* (Yale Univ. Press, New Haven, 1980).
20. Lindstrom, E. R. *et al.* Disease reveals the predator: Sarcoptic mange, red fox predation, and prey populations. *Ecology* **75,** 1042–1049 (1994).
21. O'Donoghue, M., Boutin, S., Hofer, E. J. & Boonstra, R. in *Ecosystem Dynamics of the Boreal Forest: the Kluane Project* (eds Krebs, C. J., Boutin, S. & Boonstra, R.) 325–340 (Oxford Univ. Press, New York, 2001).
22. Bulmer, M. G. A statistical analysis of the 10-year cycle in Canada. *J. Anim. Ecol.* **43,** 701–718 (1974).
23. Berryman, A. A. What causes population cycles of forest Lepidoptera? *Trends Ecol. Evol.* **11,** 28–32 (1996).
24. Ginzburg, L. R. & Taneyhill, D. E. Population cycles of forest Lepidoptera: a maternal effect hypothesis. *J. Anim. Ecol.* **63,** 79–92 (1994).
25. Thomson, D. J. Spectrum estimation and harmonic analysis. *Proc. IEEE* **70,** 1055–1096 (1982).
26. Park, J., Lindberg, C. R. & Vernon, F. L. Multitaper spectral analysis of high-frequency spectrograms. *J. Geophys. Res.* **92,** 12675–12684 (1987).
27. Lees, J. M. & Park, J. Multiple-taper spectral analysis: a stand-alone C-subroutine. *Comput. Geosci.* **21,** 199–236 (1995).

Acknowledgements

We thank C. Godfray for permission to analyse time series from the Global Population Dynamics Database (GPDD). We thank J. Fryxell, B.K. Gilbert, S. Henke, P.J. Hudson, C.J. Krebs, L. Oksanen, B. Sanderson, S. Taylor and M. Tewes for discussions on particular taxa, and J.A.J. Metz for discussions of cycle periods. The research was supported by grants from the NSF and United States Department of Agriculture (USDA).

Competing interests statement

The authors declare that they have no competing financial interests

Correspondence and requests for materials should be addressed to W.M. (e-mail: murdoch@lifesci.ucsb.edu).

Precise inhibition is essential for microsecond interaural time difference coding

Antje Brand*, Oliver Behrend*, Torsten Marquardt†, David McAlpine† & Benedikt Grothe*

* *Max Planck Institute of Neurobiology, Am Klopferspitz 18a, 82152 Martinsried, Germany*
† *Department of Physiology, University College London, Gower Street, London WC1E 6BT, UK*

Microsecond differences in the arrival time of a sound at the two ears (interaural time differences, ITDs) are the main cue for localizing low-frequency sounds in space. Traditionally, ITDs are thought to be encoded by an array of coincidence-detector neurons, receiving excitatory inputs from the two ears via axons of variable length ('delay lines'), to create a topographic map of azimuthal auditory space[1,2]. Compelling evidence for the existence of such a map in the mammalian lTD detector, the medial superior olive (MSO), however, is lacking. Equally puzzling is the role of a—temporally very precise[3]—glycine-mediated inhibitory input to MSO neurons. Using *in vivo* recordings from the MSO of the Mongolian gerbil, we found the responses of ITD-sensitive neurons to be inconsistent with the idea of a topographic map of auditory space. Moreover, local application of glycine and its antagonist strychnine by iontophoresis (through glass pipette electrodes, by means of an electric current) revealed that precisely timed glycine-controlled inhibition is a critical part of the mechanism by which the physiologically relevant range of ITDs is encoded in the MSO. A computer model, simulating the response of a coincidence-detector neuron with bilateral excitatory inputs and a temporally precise contralateral inhibitory input, supports this conclusion.

Sensitivity to ITDs, which can be in the order of only microseconds[4], requires neuronal processing with a temporal acuity far beyond that normally observed in the mammalian central nervous system. Traditionally, ITD processing in mammals and birds is explained by means of an elegant model devised by Jeffress more than 50 years ago[1]. The model assumes the existence of arrays of coincidence-detector neurons receiving excitatory inputs from the two ears. Neurons respond maximally when stimulus-evoked action potentials, phase-locked to the stimulus waveform, converge from each ear simultaneously. Different conduction delays from each ear, assumed to result from a system of delay lines, provide a means by which different coincidence-detector neurons encode different ITDs. A systematic arrangement of such delay lines is assumed to create a topographic representation of ITDs and, thus, a map of sound positions in the azimuthal plane.

For nucleus laminaris, the ITD-processing structure in birds, the existence of such an arrangement has been confirmed[5,6]. However, for the mammalian equivalent, the MSO (Fig. 1a), direct confirmation of such an arrangement is lacking. Spherical bushy cells from each cochlear nucleus provide binaural excitatory input to MSO neurons[7,8], which *in vivo* recordings demonstrate to be sensitive to ITDs[9,10]. However, MSO neurons also receive prominent

glycine-containing inputs directly onto their somata, arising mainly from the medial, and partially from the lateral, nucleus of the trapezoid body (MNTB, LNTB; Fig. 1a)[11–14]. The contribution of these inputs to ITD processing remains unknown[3,15]. To test directly the extent to which the established Jeffress model is relevant to the processing of ITDs in mammals, we recorded responses of ITD-sensitive neurons from the MSO of the Mongolian gerbil (*Meriones unguiculatus*), a rodent with well-developed low-frequency hearing. Mongolian gerbils use ITDs for low-frequency sound localization[16], and have MSO neurons that show similar ITD sensitivity to that reported for cats and dogs[10]. Iontophoretic application of glycine and its antagonist strychnine permitted the assessment of the role of inhibition in the mammalian ITD detector.

Responses were recorded from 36 low-frequency MSO neurons, of which 24 were binaurally excited. Of these, 20 neurons were sensitive to ITDs with 30–85% change in the discharge rate across the physiologically relevant range of ITDs of the gerbil (roughly ±120 μs; shaded area in Fig. 1b). Most neurons (16 of 20) responded selectively to ITDs of pure tones, 4 to ITDs of only broad-band stimuli. The response maximum (best IDT) of individual neurons was largely independent of the stimulus frequency tested (Fig. 1b), a feature consistent with the Jeffress model[9]. All neurons responded maximally to sounds leading in time at the contralateral ear (positive ITDs). Note that for the neuron in Fig. 1b, maximal response is evoked by an ITD of +200 μs, outside the physiologically relevant range of the gerbil. This was a general observation.

According to a commonly held view of the Jeffress model, ITDs are systematically represented by the activity of individual coincidence-detector neurons, creating a place code of azimuthal position by virtue of their maximum firing rates[1,2]. It is generally assumed in this scheme that response maxima of ITD functions are independent of the frequency-tuning characteristics of the neurons. However, our data do not support this view. First, plotting the response of each MSO neuron to interaurally delayed 'best-frequency' tones indicate that most neurons respond maximally outside the physiologically relevant range ($n = 16$; Fig. 2a). As a consequence, ITD functions are steepest within the physiologically relevant range, creating a maximum (and unambiguous) dynamic range for each neuron's ITD-evoked response within this range. Furthermore, the ITD that evokes the peak response is dependent on neuronal tuning for sound frequency (Fig. 2b); neurons with relatively low best frequencies respond maximally at relatively long ITDs, whereas neurons with relatively high best frequencies respond maximally at relatively short ITDs, although with slight scatter of ITD maxima of neurons with best frequencies higher than 700 Hz. This correlation between best frequency and peak ITD, which is consistent with a report from a much larger sample of neurons in the auditory midbrain[17], is highly significant ($r^2 = 0.83$). When expressed in terms of the equivalent best interaural phase difference (IPD), that is, normalized for each neuron's best frequency, the peak response occurs at a constant IPD of +0.12 cycles (s.d. ±0.043; $n = 16$). Consequently, the map of best ITDs in the MSO appears to run along the tonotopic gradient; that is, there appears to be no 'place map' of ITDs within individual frequency channels.

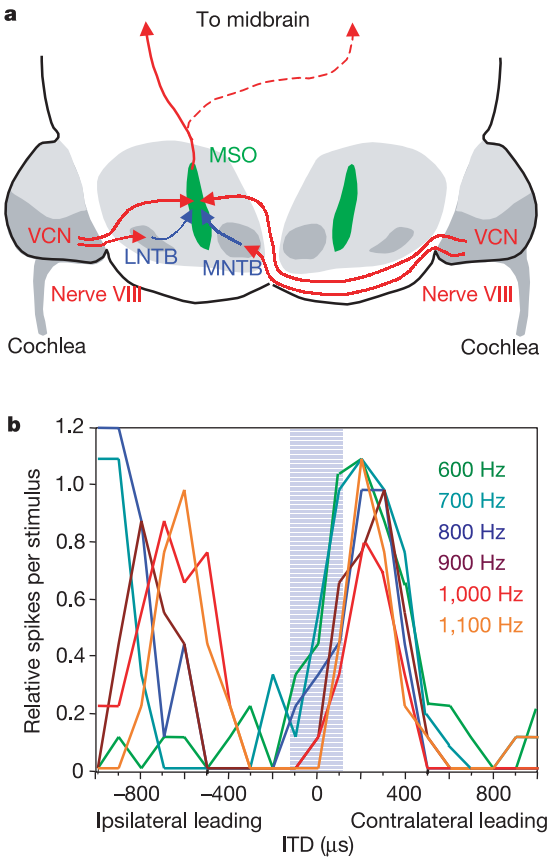

Figure 1 ITD coding in the mammalian MSO. **a**, Innervation pattern of the MSO. Excitatory inputs (red) from ventral cochlear nucleus (VCN), and glycinergic inputs (blue) from MNTB and LNTB are shown. **b**, ITD function of a gerbil MSO neuron, tested with pure tones at different frequencies. As is typical, the peak ITD is independent of stimulus frequency. The blue area indicates the physiologically relevant range for gerbils (±120 μs).

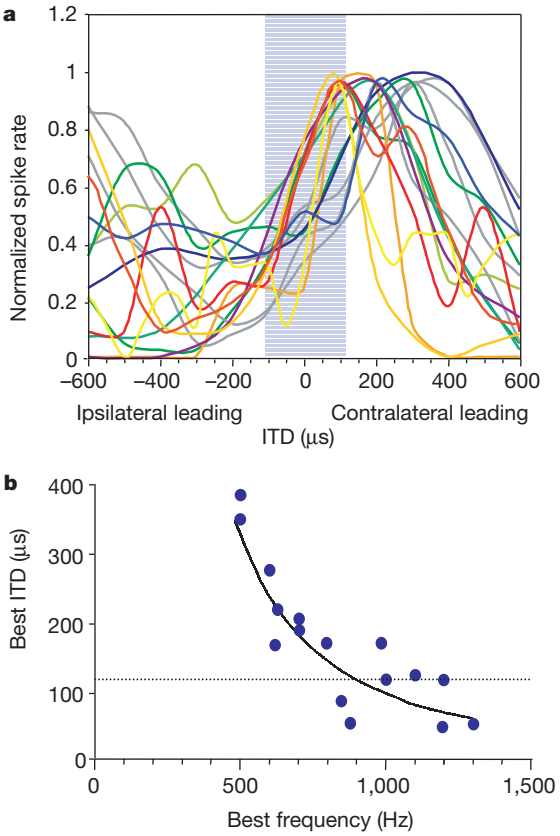

Figure 2 Peaks of ITD functions are outside of the physiologically relevant range. **a**, ITD functions of gerbil MSO neurons, each tested at its best frequency, 20 dB above threshold. Note that the peaks are largely outside the physiologically relevant range (blue area). The steep slopes of the ITD functions are within the relevant area. **b**, Distribution of best ITDs as a function of best frequencies of the neurons. Only ITDs below the dotted line are within the physiologically relevant range of ITDs. Solid line, third-order polynomial fit. Dotted line, upper limit of the gerbil's physiological range of ITDs.

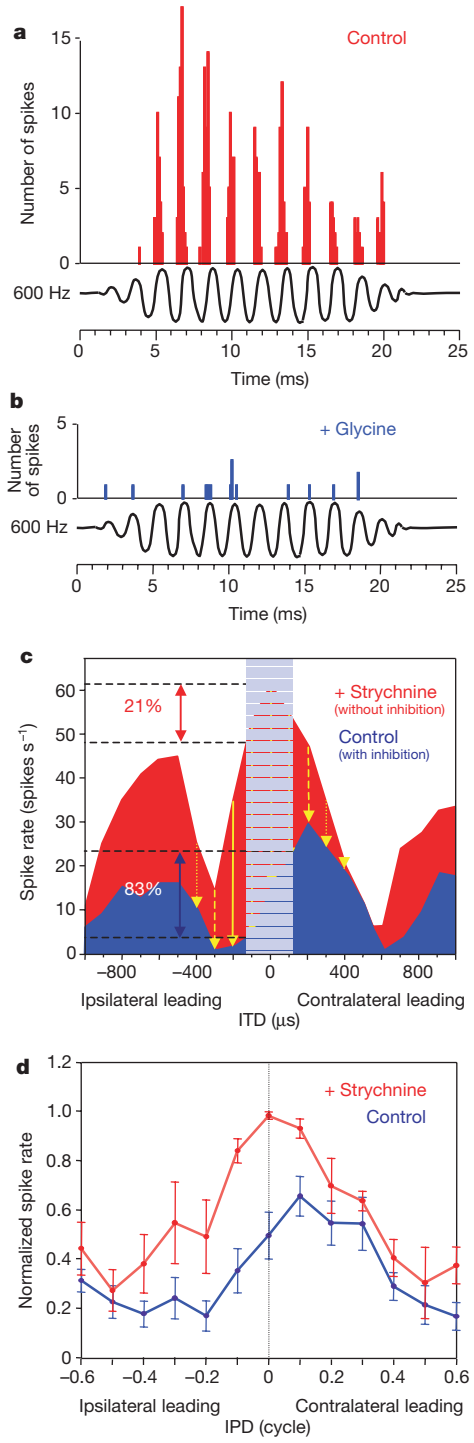

Figure 3 Effects of glycine and its antagonist strychnine in gerbil MSO neurons **a**, Peri-stimulus-time histogram showing precise phase-locking of a neuron in response to a 600-Hz pure tone. **b**, Iontophoretic application of glycine with minimal currents (<30 nA) and for only a few seconds completely inhibits the tone-evoked response. **c**, ITD functions of a neuron (best frequency 1,060 Hz) during control condition and strychnine application. Dynamic range of the ITD response under control conditions (blue) is 83%; the best ITD is outside of the physiologically relevant range (blue area). During blockade of glycinergic inhibition from application of strychnine (red), the best ITD is at zero ITD, and the dynamic range of the response is reduced to 21%. Hence, glycinergic inhibition reduces spike counts and shifts the left slope into the relevant range of ITDs. The yellow arrows indicate the different effects of inhibition at different ITDs. **d**, Averaged interaural delay functions (ITDs converted to IPD, thereby normalizing for BF) for all five ITD-sensitive neurons tested under control conditions (blue) and during application of strychnine (red). Before averaging, each neuron's IPD function was normalized to the maximal response during strychnine application (see text). Error bars, s.e.m.

The most puzzling finding in the mammalian ITD encoding circuitry is the glycinergic inhibitory input to the MSO. To determine the role of this input on ITD coding, the inhibitory transmitter glycine ($n = 5$) or its antagonist strychnine ($n = 6$) was applied during recordings made from nine MSO neurons (two neurons were successfully tested for both). For all five neurons, application of glycine almost completely abolished the response to the test tone (Fig. 3a, b) confirming the existence of glycine receptors and their profound inhibitory effect on MSO neurons.

To assess more directly the influence of glycinergic inhibition on ITD sensitivity of individual MSO neurons, we successfully applied the glycine antagonist strychnine on six neurons. Five of these neurons were sensitive to ITDs. Two effects were observed. First, in all six neurons, strychnine produced a significant increase in discharge rate (50–86% at or close to zero ITD). Second, for each of the five neurons that were ITD sensitive, application of strychnine shifted the peak of the ITD functions towards zero ITD. The blue area in Fig. 3c shows the ITD function for one of the five neurons (best frequency 1,060 Hz) under control conditions (in the absense of strychnine). The ITD function showed the typical monotonic increase of discharge rate across the relevant extent of ITDs, in this case of about 83%. The neuron's peak ITD was +170 μs, outside the physiologically relevant range for the gerbil. When strychnine was applied (red area in Fig. 3c), the best ITD shifted downwards to +50 μs, some 120 μs from its initial peak, corresponding to a shift in best IPD of 0.127 cycles. The steepest slope of the function therefore fell outside the physiologically relevant range of ITDs. In addition, the function became nonmonotonic within the physiological range and, hence, ambiguous for ITD. The dynamic range within the physiological range was reduced from 83% to 21%. In each of the five neurons tested, strychnine shifted the best ITD close to zero ITD. The mean equivalent IPD of these five neurons before application of strychnine was 0.148 cycles (±0.054) and 0.021 cycles (±0.053) during application of strychnine. Hence, strychnine caused an average shift of −0.127 cycles (±0.064) The shifts observed in all five neurons were statistically significant (paired t-test, $P < 0.014$).

The averaged IPD functions for the five neurons after first normalizing each function to the maximum discharge rate in the presence of strychnine are shown in Fig. 3d. The average function is similar to that of the example neuron in Fig. 3c. On average, iontophoresis of strychnine produced a 67% (±9.8%) reduction of the dynamic range of the response across the physiologically relevant range of ITDs. The yellow arrows in Fig. 3c indicate the apparent effect of the glycinergic inhibition, which differed at different ITDs, being stronger when the ipsilateral stimulus was leading in time than when the the contralateral stimulus was leading. Because glycinergic inputs to the MSO are insensitive to ITDs, the only explanation for this observation is that the inhibition occurs in specific phase relation to the excitatory inputs; that is, it is precisely phase-locked. To explain the influence of inhibition in shifting the peaks of ITD functions in the observed direction, one could assume ipsilaterally driven inhibition that follows (phase lags) the ipsilateral excitation, contralateral inhibition that precedes contralateral excitation, or a combination of both. However, contralateral inhibition preceding contralateral excitation is a common phenomenon in the bat MSO[18], and the contralateral inhibition has been shown to be more prominent than the ipsilateral inhibition[13,15].

The shift in ITD tuning that results from a phase-locked, contralateral inhibition preceding contralateral excitation was simulated using a modified Hodgkin–Huxley model[19] (Fig. 4) on the basis of physiological findings in neurons of the anteroventral cochlear nucleus (AVCN). AVCN neurons exhibit similar nonlinear membrane properties to those seen in the MSO. In this model, an additional voltage-dependent, low-threshold potassium channel renders the single-compartment model particularly sensitive to

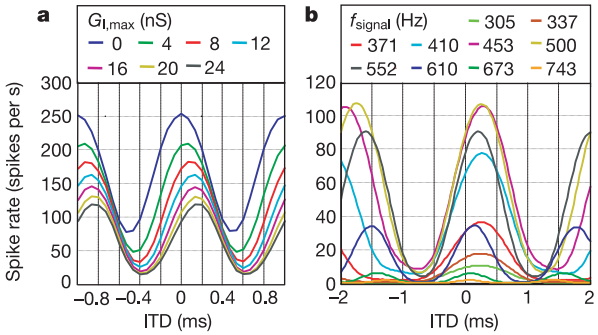

Figure 4 Simulation of the shift in ITD caused by timed contralateral inhibition using a modified Hodgkin–Huxley model (see text). **a**, ITD functions with various inhibitory synaptic strength (tuning maximum synaptic conductance, $G_{I,max}$) show the influence of the contralateral inhibition on best ITD and overall spike rate (signal frequency is 1,000 Hz). **b**, ITD functions of a simulated 500-Hz neuron to interaurally delayed tones of various frequencies. The central peak of the ITD functions is largely independent of the stimulus frequency ($G_{I,max} = 10$ nS).

the relative timing of its spike inputs. Consistent with our physiological observations (Fig 3c, d), Fig. 4a illustrates how increasing the strength (that is, conductance $G_{I,max}$) of the timed inhibition progressively shifts the central peak of the function towards longer values of ITD, and reduces the overall discharge rate. To simulate the physiological results from the stimulation frequency of 1,000 Hz (Fig. 3c), we set both the excitatory and the inhibitory synaptic time constants to $\tau = 0.1$ ms, giving a half-time of 0.25 ms (for lower test frequencies, slower time constants were sufficient). ITD functions for several stimulus frequencies are shown in Fig. 4b, for a simulated neuron with a best frequency of 500 Hz. The typical pattern of a coincidence-detector neuron is evident, with the position of the central peak largely independent of stimulus frequency, although there is a systematic tendency for the peak to shift towards lower ITDs as input level decreases, owing to peripheral auditory filtering. These results indicate that a phase-locked and precisely timed contralateral inhibition, such as innervates the MSO from the MNTB, and preceding the contralateral excitation, can account for the neural responses observed.

Our data indicate that ITD tuning in the gerbil MSO is the product of an interaction of precisely timed excitatory and inhibitory inputs. Moreover, the glycinergic inhibition appears responsible for tuning the steep slope of ITD functions to the physiologically relevant range by suppressing the response to ITDs at which the ipsilateral stimulus is leading. Because the inhibitory input is not ITD sensitive itself, the most likely explanation is that a monaural phase-locked inhibitory input is responsible for this behaviour. In fact, sources of inhibition to the MSO, from the MNTB in particular, show unique morphological and physiological specializations (including calyx synapses) that enable highly temporally precise transmission of neural signals[20,21], and strong evidence exists that the contralateral, MNTB-derived inhibition is the dominant inhibitory input to the MSO[13,15]. To influence responses to negative ITDs (ipsilateral leading), such contralateral inhibition must precede contralateral excitation. Glycinergic inhibition preceding excitation evoked from the same ear is a common phenomenon in the bat MSO[18,22]. Exact temporal adjustment of the input to the MSO from the MNTB is, therefore, crucial for creating the 'correct' ITD, as is an inhibitory time constant much faster than that observed in the rat MSO[14]. The temporal adjustment of the fast time constant, however, might be related to the experience-dependent elimination of glycinergic synapses on MSO neurons during the first days after hearing onset, refining the inputs to the MSO somata only—in contrast to the diffuse distribution in the rat[23]. The finding that inhibitory transmitters are crucial in processing ITDs (as with other temporal cues[8]), taken together with evidence for an age-related downregulation of inhibitory transmitters[24], offers new ways of explaining age-related hearing deficits, such as the deterioration of the capacity to segregate sound sources. Finally, our results provide support for a model of spatial hearing, based on recent observations in the guinea pig midbrain[17], in which the slopes of ITD functions, rather than their peaks, are the critical feature in determining how they might contribute to the localization of sound sources in azimuth. Altogether, the traditional model of low-frequency spatial hearing[1] seems not to be an adequate description of how ITDs are either encoded or represented in the mammalian auditory system. □

Methods

Sample sizes

We recorded from 36 low-frequency (<2 kHz) neurons histologically localized to the MSO, of which 20 showed a profound ITD sensitivity. It is commonly reported to be difficult to record from MSO neurons[25,9,10]. Additionally, application of glycine and particularly of its antagonist strychnine turned out to be difficult, presumably because of the high density of cell bodies in the central region of the MSO and of the densely packed myelinated MSO input and output fibres that prevented the relatively large molecule from reaching the receptors of the cells from which we recorded. Thus, only 'ideal' recording configuration allowed successful application of drugs, which explains the $n = 9$ neurons with drug application in this study.

Delivery of stimuli to animals

Animals (Mongolian gerbils, *Meriones unguiculatus*) were anaesthetized with a mixture of Ketamine (10 mg per 100 g) and Rompun (2%) throughout the entire experiment. During recordings, the animal was placed on a heating cushion in a sound-attenuated chamber. Recording electrodes were inserted stereotaxically through the foramen magnum[10]. We used glass pipettes for recordings filled with 2 M sodium acetate (impedance 10–30 MΩ) glued to a five-barrel glass electrode[26], allowing local iontophoretic application of 0.5 M glycine (10–40 nA), 0.01 M strychnine (50–250 nA), or 4% solution of horseradish peroxidase (HRP, Sigma) at the recording site. One barrel filled with sodium acetate (1 M) served as a balancing channel. Recording sites were anatomically confirmed by histological analysis of the HRP injections.

Action potentials were recorded using conventional methods described elsewhere[27]. Only action potentials from single neurons with a signal-to-noise ratio greater than five were recorded.

Stimuli were delivered using Tucker Davis Technologies (TDT) System II[27] and two Beyer dynamics speakers (model DT 990), fitted to the ears by probe tubes (2 mm inner diameter). The stimulus-delivering system and the speakers were calibrated using a 1/4-inch microphone (Reinstorp VtS), a measuring amplifier (MV 302, Microtech) and a waveform analyser (Stanford Research Systems, model SR770 FFT network analyser).

Data recording

After electrophysiological isolation of a single neuron, a frequency-tuning curve was measured and the best frequency and threshold determined. Sensitivity to static ITDs was then tested using different stimulus frequencies. For all tests during drug applications, the frequency was set to the best frequency of the neuron, 20 dB above its threshold. Stimulus duration was 100 or 200 ms, delivered at a rate of 4 stimuli s per s with at least ten repetitions. The stimulus delay was constant at the contralateral ear and varied at the ipsilateral, covering a range of up to ±1 ms (resolution of 50 or 100 μs). Data were analysed offline using individual spike times and peri-stimulus-time histograms. Also, we performed a vector analysis to evaluate the degree of phase-locking and the best ITD[25,28]. All experiments were approved according to the German Tierschutzgesetz.

Model parameters

The model is identical to one previously applied in the simulation of MSO neurons[29], and, if not otherwise stated, all parameters used here were identical, except that both the excitatory and the inhibitory synaptic time constants were short ($\tau = 0.1$ ms), giving a

half-time of 0.25 ms. The maximum excitatory conductance was $G_{E,max} = 1.5$ nS. All 2×24 excitatory and 24 inhibitory pre-synaptic inputs were generated independently by an auditory nerve model[30] that produced about 160 spikes in response to the 1-s-tone-burst stimulus when the tone's frequency equals the best frequency. The contralateral inhibition led the excitation from either side by 0.2 ms. For simplicity, the simulations of cochlear nucleus neurons and inhibitory interneurons in the trapezoid body were omitted.

Received 31 December 2001; accepted 13 March 2002.

1. Jeffress, L. A. A place theory of sound localization. *J. Comp. Physiol. Psychol.* **41,** 35–39 (1948).
2. Joris, P. X., Smith, P. H. & Yin, T. C. Coincidence detection in the auditory system: 50 years after Jeffress. *Neuron* **21,** 1235–1238 (1988).
3. Grothe, B. & Sanes, D. H. Synaptic inhibition influences the temporal coding properties of medial superior olivary neurons: an in vitro study. *J. Neurosci.* **14,** 1701–1709 (1994).
4. Klumpp, R. & Eady, H. Some measurements of interaural time difference thresholds. *J. Acoust. Soc. Am.* **28,** 215–232 (1956).
5. Overholt, E., Rubel, E. W. & Hyson, R. L. A circuit for coding interaural time differences in the chick brainstem. *J. Neurosci.* **12,** 1698–1708 (1992).
6. Carr, C. E. & Konishi, M. Axonal delay lines for time measurement in the owl's brainstem. *Proc. Natl Acad. Sci. USA* **85,** 8311–8315 (1988).
7. Smith, P. H., Joris, P. X. & Yin, T. C. Projections of physiologically characterized spherical bushy cell axons from the cochlear nucleus of the cat: evidence for delay lines to the medial superior olive. *J. Comp. Neurol.* **331,** 245–260 (1993).
8. Grothe, B. The evolution of temporal processing in the medial superior olive, an auditory brainstem structure. *Prog. Neurobiol.* **61,** 581–610 (2000).
9. Yin, T. C. & Chan, J. C. Interaural time sensitivity in medial superior olive of cat. *J. Neurophys.* **64,** 465–488 (1990).
10. Spitzer, M. W. & Semple, M. N. Neurons sensitive to interaural phase disparity in gerbil superior olive: diverse monaural and temporal response properties. *J. Neurophys.* **73,** 1668–1690 (1995).
11. Cant, N. B. & Hyson, R. L. Projections from the lateral nucleus of the trapezoid body to the medial superior olivary nucleus in the gerbil. *Hearing Res.* **58,** 26–34 (1992).
12. Kuwabara, N. & Zook, J. M. Projections to the medial superior olive from the medial and lateral nuclei of the trapezoid body in rodents and bats. *J. Comp. Neurol.* **324,** 522–538 (1992).
13. Grothe, B. & Sanes, D. H. Bilateral inhibition by glycinergic afferents in the medial superior olive. *J. Neurophys.* **69,** 1192–1196 (1993).
14. Smith, A. J., Owens, S. & Forsythe, I. D. Characterisation of inhibitory and excitatory postsynaptic currents of the rat medial superior olive. *J. Physiol.* **529,** 681–698 (2000).
15. Grothe, B. & Park, T. J. Sensitivity to interaural time differences in the medial superior olive of a small mammal, the Mexican free-tailed bat. *J. Neurosci.* **18,** 6608–6622 (1998).
16. Heffner, R. S. & Heffner, H. E. Sound localization and use of binaural cues by the gerbil (*Meriones unguiculatus*). *Behav. Neurosci.* **102,** 422–428 (1988).
17. McAlpine, D., Jiang, D. & Palmer, A. R. A neural code for low-frequency sound localization in mammals. *Nature Neurosci.* **4,** 396–401 (2001).
18. Grothe, B., Park, T. J. & Schuller, G. Medial superior olive in the free-tailed bat: response to pure tones and amplitude-modulated tones. *J. Neurophys.* **77,** 1553–1565 (1997).
19. Rothman, J. S., Young, E. D. & Manis, P. B. Convergence of auditory nerve fibers onto bushy cells in the ventral cochlear nucleus: implications of a computational model. *J. Neurophys.* **70,** 2562–2583 (1993).
20. Smith, P. H., Joris, P. X. & Yin, T. C. Anatomy and physiology of principal cells of the medial nucleus of the trapezoid body (MNTB) of the cat. *J. Neurophys.* **79,** 3127–3142 (1998).
21. Taschenberger, H. & von Gersdorff, H. Fine-tuning an auditory synapse for speed and fidelity: developmental changes in presynaptic waveform, EPSC kinetics, and synaptic plasticity. *J. Neurosci.* **20,** 9162–9173 (2000).
22. Grothe, B. Interaction of excitation and inhibition in processing of pure tone and amplitude-modulated stimuli in the medial superior olive of the mustached bat. *J. Neurophys.* **71,** 706–721 (1994).
23. Kapfer, C., Seidl, A. H., Schweizer, H. & Grothe, B. Experience-dependent refinement of inhibitory inputs to auditory coincidence-detector neurons. *Nature Neurosci.* **5,** 257–253 (2002).
24. Willott, J. F., Milbrandt, J. C., Bross, L. S. & Caspary, D. M. Glycine immunoreactivity and receptor binding in the cochlear nucleus of c57bl/6j and cba/caj mice: effects of cochlear impairment and aging. *J. Comp. Neurol.* **385,** 405–414 (1997).
25. Goldberg, J. M. & Brown, P. B. Response of binaural neurons of dog superior olivary complex to dichotic tonal stimuli: some physiological mechanisms of sound localization. *J. Neurophys.* **32,** 613–636 (1969).
26. Havey, D. C. & Caspary, D. M. A simple technique for constructing 'piggy-back' multibarrel microelectrodes. *Electroencephalogr. Clin. Neurophys.* **48,** 249–251 (1980).
27. Brand, A., Urban, A. & Grothe, B. Duration tuning in the mouse auditory midbrain. *J. Neurophys.* **84,** 1790–1799 (2000).
28. Yin, T. C. & Kuwada, S. Binaural interaction in low-frequency neurons in inferior colliculus of the cat. III. Effects of changing frequency. *J. Neurophys.* **50,** 1020–1042 (1983).
29. Brughera, A. R., Stutman, E. R., Carney, L. H. & Colburn, H. S. A model with exitation and inhibition for cells in the medial superior olive. *Audit. Neurosci.* **2,** 219–233 (1996).
30. Carney, L. H. A model for the responses of low-frequency auditory-nerve fibers in cat. *J. Acoust. Soc. Am.* **93,** 401–417 (1993).

Acknowledgements

We thank G. Breutel for technical assistance, C. Kapfer for suggestions, and M. Goetz for critical comments on the manuscript. This work was supported by the German Research Foundation (A.B., O.B., B.G.) and by the Medical Research Council (T.M., D.M.).

Competing interests statement

The authors declare that they have no competing financial interests.

Correspondence and requests for materials should be addressed to B.G. (e-mail: bgrothe@neuro.mpg.de).

Nogo-66 receptor antagonist peptide promotes axonal regeneration

Tadzia GrandPré*, Shuxin Li* & Stephen M. Strittmatter

Department of Neurology and Section of Neurobiology, Yale University School of Medicine, P.O. Box 208018, New Haven, Connecticut 06520, USA
** These authors contributed equally to this work*

Myelin-derived axon outgrowth inhibitors, such as Nogo, may account for the lack of axonal regeneration in the central nervous system (CNS) after trauma in adult mammals. A 66-residue domain of Nogo (Nogo-66) is expressed on the surface of oligodendrocytes[1] and can inhibit axonal outgrowth through an axonal Nogo-66 receptor (NgR)[2]. The IN-1 monoclonal antibody recognizes Nogo-A and promotes corticospinal tract regeneration and locomotor recovery[3–5]; however, the undefined nature of the IN-1 epitope in Nogo, the limited specificity of IN-1 for Nogo, and nonspecific anti-myelin effects have prevented a firm conclusion about the role of Nogo-66 or NgR. Here, we identify competitive antagonists of NgR derived from amino-terminal peptide fragments of Nogo-66. The Nogo-66(1–40) antagonist peptide (NEP1–40) blocks Nogo-66 or CNS myelin inhibition of axonal outgrowth *in vitro*, demonstrating that NgR mediates a significant portion of axonal outgrowth inhibition by myelin. Intrathecal administration of NEP1–40 to rats with mid-thoracic spinal cord hemisection results in significant axon growth of the corticospinal tract, and improves functional recovery. Thus, Nogo-66 and NgR have central roles in limiting axonal regeneration after CNS injury, and NEP1-40 provides a potential therapeutic agent.

Previously, we sought to determine which residues within the Nogo-66 domain are responsible for inhibition of axon outgrowth[1]. Five 25-residue peptides, consisting of overlapping segments of the Nogo-66 sequence, were assessed in axonal outgrowth assays. Only the peptide consisting of residues 31–55 is inhibitory, demonstrating the role of these residues in receptor activation. However, the inhibitory potency of this peptide is three orders of magnitude less than the entire 66-residue fragment, suggesting that regions other than residues 31–55 contribute to high-affinity binding of Nogo-66 to its receptor. To determine which Nogo-66 residues are required for high-affinity binding, we produced fusion proteins of placental alkaline phosphatase (AP) and various fragments of Nogo-66. Several of the Nogo-66 deletion mutants bind as avidly as Nogo-66 to COS7 cells expressing NgR (Fig. 1a). Notably, the deletion of residues 34–66, encompassing half of the Nogo-66 sequence, does not prevent high-affinity binding by the Nogo-66(1–33) fusion protein. Binding of the Nogo-66(1–31) fusion protein is slightly reduced (dissociation constant, $K_d = 24 \pm 11$ nM; Fig. 1a and data not shown) compared with the Nogo-66(1–33) and longer fusion proteins (K_d values $= 11–14 \pm 3$ nM). Additional deletions from the carboxyl end of Nogo-66 markedly reduce NgR binding, such that proteins containing fewer than the 31 N-terminal residues of Nogo-66 exhibit no binding to NgR under these conditions. The necessity of residues at the N terminus was tested in the setting of the Nogo-66(1–40) fusion protein. Deletion of five N-terminal residues in the Nogo-66(6–40) protein significantly reduces binding, and deletion of ten residues (Nogo-66(11–40) protein) abolishes binding. Thus, residues 1–31 seem to be sufficient for high-affinity binding to NgR. Within the N-terminal portion of Nogo-66, at least some of the first ten residues (RIYKGVIQA) and residues in the 30–33 region (SEEL) are necessary for maximal binding. The necessity of specific residues from 11–30 for high-affinity binding is not tested here.